Aberro-polariscope for the human eye

Juan M. Bueno, Esther Berrio, and Pablo Artal

Laboratorio de Óptica, Departamento de Física, Universidad de Murcia, Campus de Espinardo (Edificio C), 30071 Murcia, Spain

Received January 22, 2003

We have developed an aberro-polariscope that simultaneously measures spatially resolved polarization properties and wave-front aberration in a living human eye. The setup consists of an infrared Hartmann–Shack sensor that incorporates a polariscope. A series of four Hartmann–Shack images corresponding to independent polarization states were recorded. The corresponding wave-front aberration was computed from each image. Moreover, from each set of four images spatially resolved (over the pupil plane) parameters of polarization were also determined. This instrument allows useful information on both the optical and the biomechanical properties of the eye to be obtained. © 2003 Optical Society of America

OCIS codes: 120.5410, 170.3880, 330.5370, 330.7310.

Although the imaging and biomechanical properties of the human eye are closely related, they have traditionally been studied separately. In recent years, since a better understanding of refractive surgery has been required, there has been a growing need for new instruments that can obtain both optical and biomechanical information about the eye.

Concerning the quality of retinal images in the human eye, many different techniques have been developed to measure aberrations.[1–3] However, the most widely used instrument today is the Hartmann–Shack (HS) wave-front sensor.[4,5]

On the other hand, polarimetry can provide information on ocular biomechanics. Different imaging polarimetric methods have been applied to the eye in past studies.[6–8] Polariscopes[9–11] are used when birefringence is the dominant polarization property in a system (such as the eye)[6,8,12–14] and the complete Mueller matrix is not required. In this Letter we present an instrument that combines spatially resolved polarimetry and wave-front sensing for the eye.

Figure 1 shows a schematic diagram of the apparatus. A polariscope composed of a fixed linear vertical polarizer (P1) in the generator unit and a rotatory $\lambda/4$ retarder and another vertical polarizer (P2) in the analyzer unit was incorporated into a HS wave-front sensor. A collimated infrared laser beam (1.5 mm in diameter) was used as a beacon light source. The use of infrared light increases the amount of light reflected by the retina and is more comfortable for the subjects. The light beam passes P1 before entering the eye. In the exit pathway two achromatic doublets (L1 and L2) optically conjugate the pupil's plane with the microlens array (ML). Two mirrors (M3 and M4) mounted on a moving stage were used as a focus-corrector stage (FC) in a Badal optometer configuration. The light emerging from the eye passes the focus corrector and the analyzer unit. Finally, the beam is sampled by the array of microlenses and focused on a CCD camera that records the HS images. The head of the subject was stabilized with a bite bar mounted on a three-axis positioning stage. An additional video camera (CP) controls the correct position of the subject's natural pupil during exposures. By orienting the fast axis of the $\lambda/4$ retarder at four different angles ($-45°$, $0°$, $30°$, and $60°$), four independent polarization states are produced in the analyzer unit.[15] One HS image was recorded for each orientation. The complete experimental system was first calibrated to verify its reliability as described elsewhere.[13] The apparatus barely depolarizes the light (degree of polarization, 0.97), and the residual retardation introduced is smaller than 3°.

Series of four HS images (500-ms exposure time) were recorded for four eyes (two right, two left) from four normal (having neither ocular pathologies nor prior history of refractive surgery) young-adult subjects with natural pupil sizes. The wave-front aberration was calculated for each individual HS image as previously described.[5] In addition, for each set of four images the elements of the Stokes vector associated with the polarization state of the light emerging from the eye was calculated for each spot in the HS image. This provided a spatial resolution limited by the size of each spot. Parameters of polarization such as the degree of polarization (DOP) and the retardation (δ) and azimuth of the fast axis (α) related to the ocular birefringence were extracted from this vector. These were computed as follows.

Let S_{OUT} be the Stokes vector emerging from the eye. If M_{PSA} is an auxiliary 4×4 matrix with each

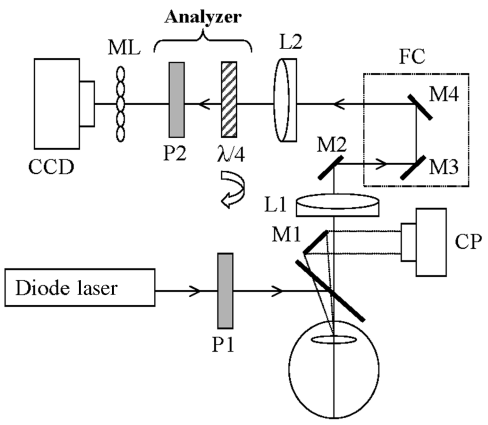

Fig. 1. Simplified schematic diagram of the aberro-polariscope. See text for further details.

0146-9592/03/141209-03$15.00/0

row being the first row of every Mueller matrix corresponding to an independent polarization state in the analyzer unit, then it is verified that

$$\begin{pmatrix} I_1 \\ I_2 \\ I_3 \\ I_4 \end{pmatrix} = \frac{1}{2}\begin{bmatrix} 1 & 0 & 0 & -1 \\ 1 & -1 & 0 & 0 \\ 1 & -1/4 & -\sqrt{3}/4 & \sqrt{3}/2 \\ 1 & -1/4 & \sqrt{3}/4 & \sqrt{3}/2 \end{bmatrix} \times \begin{pmatrix} S_0 \\ S_1 \\ S_2 \\ S_3 \end{pmatrix} = M_{\mathrm{PSA}} S_{\mathrm{OUT}}, \quad (1)$$

where I_j ($j = 1, 2, 3, 4$) are the averaged intensities of one spot in the four HS images.

The elements of S_{OUT} can be calculated by inversion of Eq. (1):

$$S_{\mathrm{OUT}} = \begin{pmatrix} S_0 \\ S_1 \\ S_2 \\ S_3 \end{pmatrix} = (M_{\mathrm{PSA}})^{-1} \begin{pmatrix} I_1 \\ I_2 \\ I_3 \\ I_4 \end{pmatrix}. \quad (2)$$

This vector contains information on δ, α, and the depolarization caused by ocular structures. In particular, the DOP can be directly computed from Eq. (2) as

$$\mathrm{DOP} = \frac{({S_1}^2 + {S_2}^2 + {S_3}^2)^{1/2}}{S_0} \qquad (0 \le \mathrm{DOP} \le 1). \quad (3)$$

Since ocular birefringence has been reported to be linear,[8,13–15] and considering the expressions of the Mueller matrix for an optical system containing properties of birefringence and depolarization,[16] δ and α at each spot in the HS image can be obtained from

$$\alpha = \frac{1}{2}\, a\tan\left(-\frac{\mathrm{DOP} + S_1}{S_2}\right)$$

$$\delta = \mathrm{a}\cos\left[1 + \frac{2S_2}{\mathrm{DOP}\,\sin(4\alpha)}\right]. \quad (4)$$

As an example, results for the right eye of one of the subjects are presented here. Figure 2 shows the HS images and the associated aberrations. As previously reported,[17,18] the aberrations were similar, and the image quality in the eye is nearly independent of the state of polarization. The corresponding averaged root-mean-square errors (from the third to the sixth Zernike order and 5-mm pupil) were 0.29 ± 0.02, 0.37 ± 0.02, 0.35 ± 0.02, and 0.33 ± 0.01.

The spatially resolved DOP for the same subject calculated with Eq. (3) is presented in Fig. 3. For the set of subjects used here the maximum value for the DOP ranged from 0.65 to 0.90. Although this maximum was not always located at the center of the pupil, the DOP was reduced toward the margin of the pupil. These results agree with previous experiments.[19,20] Moreover, the location of the maximum for the DOP could be associated with the peak of the Stiles–Crawford effect,[19] which in many subjects can be at a location other than the center of the pupil. Lower values of this parameter correspond to light scattered in the ocular media. In this sense the DOP can also be used to measure the directional properties of photoreceptors.

Maps of δ and the slow axis (90° apart from α) are shown in Figs. 4 and 5 for the same subject. The incidence was perpendicular to the center of the cornea and the beam came to a single point at the foveola (~5 arc min). This area is free of nerve fibers and has only a small birefringence because the Henle fiber layer is present. Since the associated retardation is up to 10 times smaller than that of the cornea,[6,12] we can assume that the cornea is mainly responsible for the retardation. Whereas δ contains information on changes in corneal thickness and local disturbances in corneal structure, α contains information on the distribution of the corneal stroma and the directions of stress or tensions. These results show that corneal retardation increases from the center to the periphery, probably because of an increase in both corneal thickness and birefringence toward the limbus. Although the orientation of the slow axis depends on the subject,

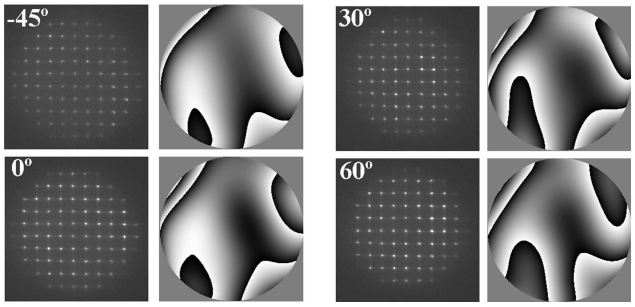

Fig. 2. HS images and associated wave-front aberration maps (calculated for a 5-mm pupil) for each of the four independent polarization states in the analyzer unit.

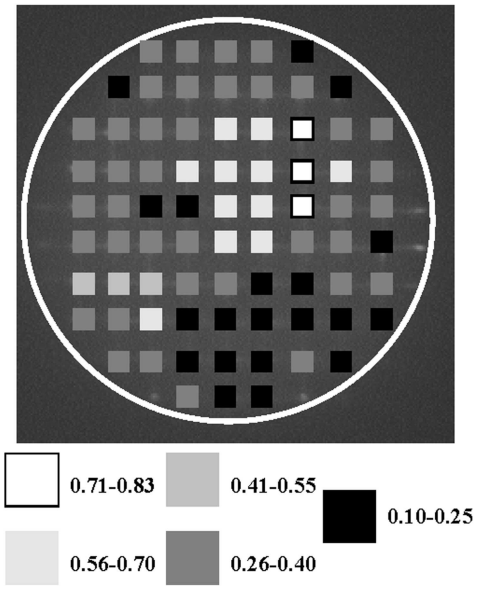

Fig. 3. Spatially resolved DOP for the right eye of a normal young-adult subject (26-year-old). The gray scale is shown at the bottom. The inserted circle corresponds to a 6.4-mm pupil size.

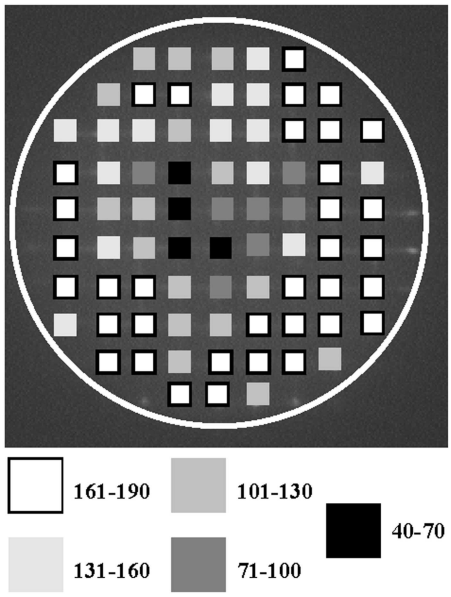

Fig. 4. Distribution of δ (spot by spot) in the same eye as in the previous figures. The corresponding gray scale is at the bottom. Units are degrees.

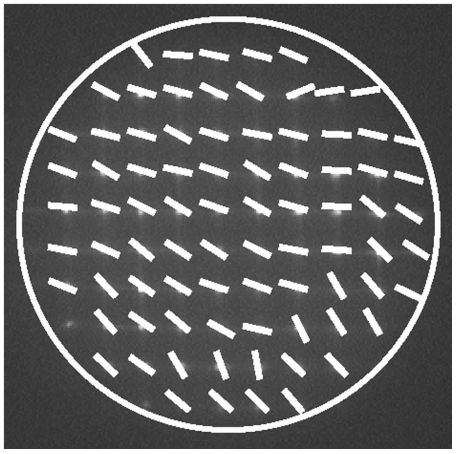

Fig. 5. Orientation of the corneal slow axis for the same right eye as in the previous figures.

it is oriented, in general, nasally downward ($-28°$ and $-12°$ for the right eye and 5° and 12° for the left eye).

In summary, we have designed, built, and tested an aberro-polariscope to simultaneously measure imaging and polarization properties in a living human eye. Unlike Mueller-matrix polarimetry, our method allows the calculation of ocular polarization parameters with a reduced number of images. Our experimental system could be further improved if the rotatory $\lambda/4$ retarder is changed by faster electro-optical modulators. Implementation of this instrument in ophthalmologic instruments could improve diagnosis techniques. In particular, the use of this setup in measuring physical changes produced by ocular surgery (LASIK, corneal transplantation) would be of interest in clinical environments.

This research was supported by the Spanish Ministry of Science and Technology, grant BFM2001-0391. J. M. Bueno's e-mail address is bueno@um.es.

References

1. M. S. Smirnov, Biofizika **6,** 776 (1961).
2. H. C. Howland and B. Howland, J. Opt. Soc. Am. **67,** 1508 (1977).
3. I. Iglesias, E. Berrio, and P. Artal, J. Opt. Soc. Am. A **15,** 2466 (1998).
4. J. Liang, B. Grimm, S. Goelz, and J. F. Bille, J. Opt. Soc. Am. A **11,** 1949 (1994).
5. P. M. Prieto, F. Vargas-Martín, S. Goelz, and P. Artal, J. Opt. Soc. Am. A **17,** 1388 (2000).
6. B. Pelz, C. Weschenmoser, S. Goelz, J. P. Fischer, R. O. Burk, and J. F. Bille, Proc. SPIE **2930,** 92 (1996).
7. J. M. Bueno and P. Artal, Opt. Lett. **24,** 64 (1999).
8. A. W. Dreher, K. Reiter, and R. N. Weinreb, Appl. Opt. **31,** 3730 (1992).
9. R. Oldenbourg and G. Mei, J. Microsc. **180,** 140 (1995).
10. J. W. Jaronski and H. T. Kasprzak, Appl. Opt. **38,** 7018 (1999).
11. J. M. Bueno and F. Vargas-Martín, Appl. Opt. **41,** 116 (2002).
12. G. J. van Blokland and S. C. Verhelst, J. Opt. Soc. Am. A **4,** 82 (1987).
13. J. M. Bueno, Vision Res. **40,** 3791 (2000).
14. G. J. van Blokland, J. Opt. Soc. Am. A **2,** 72 (1985).
15. J. M. Bueno and J. W. Jaronski, Ophthalmic Physiol. Opt. **21,** 384 (2001).
16. S. Lu and R. A. Chipman, J. Opt. Soc. Am. A **13,** 1106 (1996).
17. J. M. Bueno and P. Artal, J. Opt. Soc. Am. A **18,** 489 (2001).
18. P. M. Prieto, F. Vargas-Martín, J. S. McLellan, and S. A. Burns, J. Opt. Soc. Am. A **19,** 809 (2002).
19. J. M. Bueno, Vision Res. **41,** 2687 (2001).
20. S. A. Burns, S. Wu, F. Delori, and A. E. Elsner, J. Opt. Soc. Am. A **12,** 2329 (1995).